

Projector Methods Applied to Numerical Integration

of the S_N Transport Equation in X-Y Geometry

V. Hristea and St. Covaci

Institute for Nuclear Research PO Box 0300 Pitesti, Romania

(Received January 17, 2002)

Abstract – *We are developing two methods of integration for the S_N transport equation in X-Y geometry, methods based on projector technique. By cellularization of the phase space and by choosing a finite basis of orthonormal functions, which characterize the angular flux, the non-selfadjoint transport equation is reduced to a cellular automata. This automata is completely described by the transition Matrix T . Within this paper two distinct methods of projection are described. One of them uses transversal integration technique. As an alternative to this we apply the method of the projectors for the integral S_N transport equation. We show that the constant spatial approximation of the integral S_N transport equation does not lead to negative fluxes. One of the problems with projector method, respectively the appearance of numerical instability for small intervals, is solved by the Padé representation of the elements for Matrix T . Numerical tests here presented compare the numerical performances of the algorithms obtained through the two projection methods. The Padé representations was also taken into account for these two algorithm types.*

I Introduction

The discretisation methods of the non-selfadjoint S_n transport equation in x-y geometry is based on cellularisation of the phase space. Preliminary operations are to choose a regular network of rectangles, which are homogeneous, as well as to choose a set of discrete ordinates. The main problems that may occur for the numerical algorithms based on projector method are: negative flux's appearance, ray effect, spatial oscillations and numerical instabilities that appear for small space intervals (the void case). The negative fluxes appear not only in the case of the **DD** diamond difference

schema but also in that of nodal S_N transport algorithms. The analysis of this problem for the nodal algorithms is difficult owing to that they are presented in an implicit form (Walters and O' Dell, 1982).

The purpose of this paper is to offer a mathematical procedure based on projection technique to solve the S_N transport equation. In comparison with other treatment of the discretisation of the transport equation, the method proposed here must be developed into two directions. One of them is known as nodal and it is based on the transverse integral method (Walters and O' Dell, 1982). Another direction consists in projecting the integral S_N transport equation. The transport algorithms are mathematical objects that can be compared. To describe the algorithm derived in this paper we use the cellular automata formalism.

In Section II we propose a symbolic method for the representation of the S_N transport algorithms based on the projector method. At the basis of the representation is the notion of "cellular automata". To each cell of the phase space we associate a cellular automata. For a concise writing of the algorithms we propose a symbolical notation, which will allow writing the formulas in a compact way. We simplify the definition of the automata used in a previous paper (Hristea and Pavelescu, 1998^[1]). Instead of the two matrixes, we shall use only one, called the transition Matrix **T**.

In Section III we develop the projector method starting from the method of the transversal integration. In this way we can generalize the nodal method (Walters and O' Dell, 1982) to another spatial approximations. The principle to obtain the transition matrix consists in the multiplication of two matrixes. Throughout this paper only two spatial approximations are discussed: the constant-constant **CC** (constant on frontiers and constant inside the cell) and constant-linear **CL** (constant on frontiers and linear inside the cell). We exemplify the calculus for the **CL** approximation in Appendix A. Since through transversal integration a set of differential equations is obtained which is solved similarly to the transport equation in slab geometry, the method is denoted in the following as Green transition matrix method **GTMM**. During the analysis of the transition **T** matrix we find some interesting properties. We respond to the problem of the appearance of the negative flux. We conclude that **GTMM** transition matrix is not stochastic (Sinai, 1992) and consequently the negative flux may appear.

Another consequence comes from the Padé [1/1] development of the spatial attenuation factors that occur in the elements of **T** matrix for **CC** and **CL** approximations. We shall demonstrate through calculations that in the case of Padé representation [1/1] the two spatial approximations are equivalent

to the **DD** diamond difference schema. An extended analysis of the **GTMM** approximations is done in a previous paper (Hristea, 1999).

The integration principle along the neutrons' direction may be respected quitting the transversal integration method. In Section IV we propose the use of the integral S_N transport equation for obtaining the **T transition matrix**. This method of integration will be called throughout this paper **ITMM** (Integral Transition Matrix Method). We shall develop only two approximations for this method: constant - constant **CC** and constant - linear **CL**.

In the case of optical path tending to zero we can also apply for **ITMM** algorithms the diagonal rational Padé development of the spatial attenuation factors. For this method the case of the streaming of the neutrons in vacuum is separately treated. We have established an empirical limit for the diagonal Padé' representation order of the **ITMM** linear algorithms.

The purpose of the numerical tests presented in Section V is the analysis of the numerical performances of the **GTMM** and **ITMM** algorithms. For very thin intervals both **ITMM** and **GTMM CL** algorithms fail to converge. For this reason we also tested the algorithms obtained through the Padé' representation for **ITMM** and **GTMM** algorithms. We chose two distinct categories of benchmark problems. The first contains a nearly voided region. The other benchmark is the Stepanek test problem. We solve the fixed source as well as the eigenvalue problem. For the inner value problem the **GTMM CL** scheme proves to be the best for reaching the reference eigenvalue.

II The explicit representation of the schemes based on projector method

The projector method is simple from a mathematical point of view but the explicit writing of the algorithms requires a clear way for the calculation representation. The basis for representing the algorithms for numerical integration of the non-selfadjoint transport equation is the network of cell automata. To simplify the notations and to compactly write the algorithms analyzed within this paper it is necessary to non-ambiguously presenting the notions used.

The starting point is the discretisation of the Boltzmann equation in homogenous spatial cells. In this paper we used the S_N discrete ordinates angular approximation. The projector method is applied to the transport equation both for its integral and differential form in each cell within the phase space.

The geometry of the cell within the phase space along with the notations used from now on is

presented in Fig. 1. For each spatial cell we choose the coordinates system with its origin in the center of the spatial interval, so the projections of the angular direction $\hat{\Omega}_n$ on the two axes of coordination are positive. In this way the coordinates system for the four octants changes correspondingly.

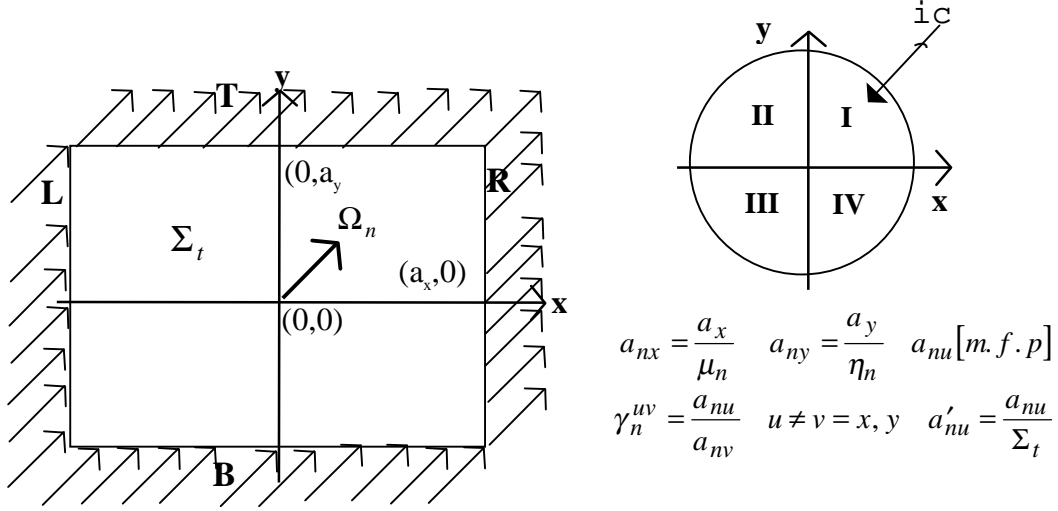


Fig. 1 Cell's geometry $\Delta x \times \Delta y \times \Delta \Omega_n$

The mono-energetic S_N transport equation normated on the total cross section both differential and integral (Lewis and Miller Jr., 1984) is:

$$(\mu_n \partial_x + \eta_n \partial_y + 1) \psi_n(x, y) = \frac{S_n(x, y)}{\Sigma_t} \equiv q_n(x, y), \quad \psi_n(x, y) = \psi_n^{in} e^{-r} + \int_0^r dr' q_n(\vec{r}') e^{-r'} \quad (1)$$

The scaling of the transport equation for the total cross section has as consequence the decrease of the number of parameters on which the solution depends, but at the same time it requires a separate treatment for the case in which section tends to zero.

From the integral form of the transport equation we notice that the solution is determined if we know the angular flux at the incoming **L** and **B** frontiers as well as the source within the spatial cell (see Figure 1). As we iterate on the scattering source, the guess flux is zero or it has a uniform positive value and the incoming fluxes at the frontiers of the problem are zero. It is clearly intuitive that we can associate a cell automata to each cell of the phase space for solving the non-autodjoint transport equation. Numerical solution through projection requires the choosing of an approximation for the fluxes at the borders and within the cell.

For defining the function spaces we use Legendre orthonormal polynomial basis. We shall associate a certain cell automata to each discrete ordinate as well as to each spatial cell (Hristea and Pavelescu, 1998^[1]). For each frontier we shall choose a system of coordinates whose orientation coincides with the orientation of the axes within the cell

The generalization of nodal algorithms requires the introduction of a set of symbols through which we can compactly write the calculation formulas for the algorithms based on the transversal integration method. We shall define the following symbol set:

$$"•" \rightarrow \psi_n(x, y) \equiv \psi_n^{••}, "+" \rightarrow \psi_n(+a_x, y) \equiv \psi_n^{+•}, \psi_n(x, +a_y) \equiv \psi_n^{•+}, "-" \rightarrow \psi_n(-a_x, y) \equiv \psi_n^{-•}, \psi_n(x, -a_y) \equiv \psi_n^{•-} \quad (2)$$

We define also the test function spaces that approximate the fluxes on the frontiers and the duals whose basis vectors are transversal projection operators:

$$\begin{aligned} \mathbf{T}_x^{\pm(L)} &\equiv \text{span}\{|0 \pm\rangle, \dots, |L-1 \pm\rangle\}, \quad \mathbf{T}_y^{\pm(L)} \equiv \text{span}\{|\pm 0\rangle, \dots, |\pm L-1\rangle\}, \quad U^{(2L)} = \mathbf{T}_x^{-(L)} \times \mathbf{T}_y^{-(L)}, \\ Q^{(2L)} &= \mathbf{T}_x^{+(L)} \times \mathbf{T}_y^{+(L)}, \quad \mathbf{T}_x^{*(L)} \equiv \text{span}\{\langle \bullet 0|, \dots, \langle \bullet L-1|\}, \quad \mathbf{T}_y^{*(L)} \equiv \text{span}\{\langle 0 \bullet|, \dots, \langle L-1 \bullet|\} \\ |k \pm\rangle &\equiv \tilde{P}_k(x), \quad |\pm l\rangle \equiv \tilde{P}_l(y), \quad \langle \bullet j| \equiv \frac{1}{2a_y} \int_{-a_y}^{a_y} dy P_j(y) \circ, \quad \langle i \bullet| \equiv \frac{1}{2a_x} \int_{-a_x}^{a_x} dx P_i(x) \circ \end{aligned} \quad (3)$$

The polynomials $\tilde{P}_l(u)$ are orthonormal Legendre ones (Hristea and Pavelescu, 1998^[2]). The space of the states $\mathbf{X}^{(M)}$ along with its dual have the following definition:

$$\begin{aligned} \mathbf{X}^{(M)} &\equiv \text{span}\{|00\rangle, \dots, |IJ\rangle\}, \quad |ij\rangle \equiv \tilde{P}_i(x) \tilde{P}_j(y), \quad M = \dim \mathbf{X}^{(M)}, \quad \psi_n^{••} \equiv |\psi_n\rangle = \sum_{i,j} \psi_n^{ij} |ij\rangle \\ \mathbf{X}^{*(M)} &\equiv \text{span}\{\langle 00|, \dots, \langle IJ|\}, \quad \langle ij| \equiv \frac{1}{2a_x 2a_y} \int_{-a_x}^{a_x} dx \tilde{P}_i(x) \int_{-a_y}^{a_y} dy \tilde{P}_j(y) \end{aligned} \quad (4)$$

The above definitions of the cellular automata (Hristea and Pavelescu, 1998^[2]) can be simplified by considering the entrance and exit spaces: $\mathbf{V}^{(P)}$ $\mathbf{W}^{(P)}$ and the transition matrix \mathbf{T}_n . The cell automata is now a 3-uple:

$$\mathbf{A}_n \equiv (\mathbf{V}^{(P)}, \mathbf{W}^{(P)}, \mathbf{T}_n), \quad \mathbf{V}^{(P)} = \mathbf{U}^{(2L)} \times \mathbf{X}^{(M)}, \quad \mathbf{W}^{(P)} = \mathbf{Q}^{(2L)} \times \mathbf{X}^{(M)}, \quad \mathbf{T}_n \equiv \begin{bmatrix} \mathbf{TRF}_n \\ \mathbf{TRZ}_n \end{bmatrix}, \quad P = 2L + M \quad (5)$$

III Transversal integration method

III A. Projection operator algebra - For the linear approximation the transversal integration method is also called "nodal" (Walters and O' Dell, 1982). This method can be extended to higher spatial approximations. The derivation formula follows a specific clear rule. The first operation consists in the transversal projection along the x and respectively y directions of the transport equation (1). We

can thus obtain a set of ordinary differential equations similar to the S_N transport equation in slab geometry. Each of these equations is integrated through the **GMM** approximation (Hristea and Pavelescu, 1998^[1]).

The next step consists in projecting the transport equation (1) by the projection operators within the dual space $X^{*(M)}$. We shall obtain a set of algebraic equations that have as unknowns the spatial moments of the flux. We generate a matrix equation and through solving it we obtain the transition matrix.

The technique of applying the projection operators becomes very simple due to the Legendre polynomials' recurrence properties:

$$DP_{n+1}(x) - DP_{n-1}(x) = (2n+1)P_n(x), \quad D\tilde{P}_m(x) = \sqrt{2m+1}(\sqrt{2(m-1)+1}\tilde{P}_{m-1}(x) + \sqrt{2(m-3)+1}\tilde{P}_{m-3}(x) + \dots) \quad (6)$$

By applying the transversal projection operators to a function with x and y variables we get taking into account notation (2):

$$\langle \bullet j | f^{\bullet\bullet} \equiv f^{\bullet j}, \quad \langle i \bullet | f^{\bullet\bullet} \equiv f^{i\bullet}, \quad f^{\bullet j} \equiv \sum_{i=0}^L f^{ij} | i \bullet \rangle, \quad f^{i\bullet} \equiv \sum_{j=0}^L f^{ij} | \bullet j \rangle \quad (7)$$

We apply the transversal projection operators to the transport equation (1). Taking into account the recurrence relation (6) we obtain:

$$\begin{aligned} \langle \bullet j | \partial_x \psi_n^{\bullet\bullet} &\equiv D_x \psi_n^{\bullet j}, \quad \langle i \bullet | \partial_y \psi_n^{\bullet\bullet} \equiv D_y \psi_n^{i\bullet}, \\ \langle \bullet j | \partial_y \psi_n^{\bullet\bullet} &\equiv \frac{\sqrt{2j+1}}{2a_y} \left[\psi_n^{+j} - \psi_n^{-j} + (1 + (-1)^{j+1}) \psi_n^{\bullet-} - 2(\sqrt{2j-1} \psi_n^{\bullet j-1} - \dots) \right], \\ \langle i \bullet | \partial_x \psi_n^{\bullet\bullet} &\equiv \frac{\sqrt{2i+1}}{2a_x} \left[\psi_n^{i+} - \psi_n^{i-} + (1 + (-1)^{i+1}) \psi_n^{-\bullet} - 2(\sqrt{2i-1} \psi_n^{i-1\bullet} - \dots) \right] \end{aligned} \quad (8)$$

By applying the 2L transversal projection operators to the transport equation (1) we obtain:

$$\begin{cases} \dots \\ \mu_n D_x \psi_n^{\bullet j} + \psi_n^{\bullet j} = q_n^{\bullet j} - \eta_n \langle \bullet j | \partial_y \psi_n^{\bullet\bullet} & \text{(a)} \\ \dots \\ \eta_n D_y \psi_n^{i\bullet} + \psi_n^{i\bullet} = q_n^{i\bullet} - \mu_n \langle i \bullet | \partial_x \psi_n^{\bullet\bullet} & \text{(b)} \\ \dots \end{cases} \quad (9)$$

The first step consists in finding the moments of the angular flux at the exit frontiers. We shall obtain an algebraic system whose unknowns are the components of the $[\Psi_n^{out}]$. These procedures can be summarized introducing the projectors $\langle +i |_G, \langle j+ |_G$. By applying these to transport operator we obtain the spatial moment of the angular flux on the outgoing frontiers **R** and **T**.

We add *at* these algebraic equations the system obtained applying the projector operators of the $x^{*(M)}$ space. The rules for the $x^{*(M)}$ projectors are:

$$\begin{aligned} \langle i \bullet | \langle \bullet j | \partial_y \Psi_n^{\bullet\bullet} &\equiv \frac{\sqrt{2j+1}}{2a_y} \left[\Psi_n^{i+} + (-1)^{j+1} \Psi_n^{i-} - 2(\sqrt{2j-1} \Psi_n^{ij-1} \dots) \right], \\ \langle i \bullet | \langle \bullet j | \partial_x \Psi_n^{\bullet\bullet} &\equiv \frac{\sqrt{2i+1}}{2a_x} \left[\Psi_n^{+j} + (-1)^{i+1} \Psi_n^{-j} - 2(\sqrt{2i-1} \Psi_n^{i-1j} \dots) \right] \end{aligned} \quad (10)$$

We obtain the matrix equation:

$$\mathbf{A}_n \left[\Psi_n^{out} \right] = \mathbf{B}_n \left[\Psi_n^{in} \right] \Rightarrow \mathbf{T}_n \equiv \mathbf{A}_n^{-1} \mathbf{B}_n \quad (11)$$

The elements of the transition matrix \mathbf{T}_n depend on two dimensionless parameters: a_{nx} and a_{ny} . The explicit method of presenting the algorithms offer the advantage of making obvious some properties of the nodal transport algorithms through the analysis of the transition \mathbf{T}_n matrix elements. We shall further on present the main properties of the numerical integration algorithms based on the transversal projection method of the S_N transport equation in x-y geometry.

III B Qualitative analysis of the GTMM algorithms - We shall next treat two types of **GTMM** spatial approximations in order to exemplify the projector method described in the above section. The **GTMM** transport algorithm for constant approximation has been previously presented (Hristea and Pavelescu, 1998^[1]). In this paper we shall continue the analysis of this approximation having for basis the representation through the transition T_n matrix. The most important notice is the one that the **GTMM CC** algorithm may lead to negative fluxes. That can be made evident by analyzing the dependence of the \mathbf{T}_n matrix elements on the parameters a_{nx} and a_{ny} .

Since we operate through the normated transport equation for the total section, it is necessary to analyze the development of the spatial attenuation factors in Padé rational fractions (Baker Jr. & Graves-Moris, 1989). We obtain the elements of the transition \mathbf{T}_n matrix as a rapport of polynomials with variables a_{nx} and a_{ny} . This way we eliminate 0/0 indeterminacy. This procedure of treating the small-dimension intervals is different from the classical method (Walters and O' Dell, 1982). More than that, we establish for the Pade' representation [1/1] that the **GTMM CC** and **CL** algorithms obtained are equivalent to the diamond difference schema **DD**.

A) GTMM CC constant approximation -The cell automata that characterize this approximation is:

$$\mathbf{A}_n^{CC} \equiv (\mathbf{V}^{(3)}, \mathbf{W}^{(3)}, \mathbf{T}_n^{CC}), [\Psi^{out}] = \mathbf{T}_n^{CC} [\Psi^{in}], [\Psi^{in}] = [\psi_n^{-0} \quad \psi_n^{0-} \quad q_n^{00}], [\Psi^{out}] = [\psi_n^{+0} \quad \psi_n^{0+} \quad \psi_n^{00}]$$

(12)

The procedure of deriving the transition matrix is described in detail in a previous paper (Hristea and Pavelescu, 1998^[2]). Using the diamond and balance relations we obtain also the transition matrix for the **DD** scheme:

$$\mathbf{T}_n^{CC} = \frac{1}{1 - e_n^y e_n^y} \begin{bmatrix} e^{-2a_{nx}} - e_{nx}^y e_n^y & 2a_{nx} e_{nx}^0 e_{ny}^0 & 2a_{nx} e_{nx}^0 g_{ny}^{00} \\ 2a_{ny} e_{nx}^0 e_{ny}^0 & e^{-2a_{ny}} - e_{nx}^0 e_{ny}^0 & 2a_{ny} g_{nx}^{00} e_{ny}^0 \\ e_{nx}^0 g_{ny}^{00} & e_{ny}^0 g_{nx}^{00} & g_{nx}^{00} g_{ny}^{00} \end{bmatrix}, \mathbf{T}_n^{DD} = \frac{1}{\Delta_n^{DD}} \begin{bmatrix} \gamma_n^{yx} - 1 - a_{ny} & 2 & 2a_{ny} \\ 2\gamma_n^{yx} & 1 - \gamma_n^{yx} - a_{ny} & 2a_{ny} \\ \gamma_n^{yx} & 1 & a_{ny} \end{bmatrix} \quad (13)$$

$$e_{nu}^0 = \frac{1 - e^{-2a_{nu}}}{2a_{nu}}, g_{nu}^{00} = 1 - e_{nu}^0, \Delta_n^{DD} = 1 + \gamma_n^{xy} + a_{ny}, \gamma_n^{uv} = \frac{a_{nu}}{a_{nv}} = \frac{a'_{nu}}{a'_{nv}}$$

The link between the **GTMM CC** and **DD** scheme can be obtained by using the diagonal Padé' [1/1] approximation of the spatial attenuation factors $\exp(-2a_{un})$ and $\exp(-2a_{uy})$. We shall check the following assertion through calculation:

Proposition 1 The **GTMM CC** cell automata in Padé' representation of the spatial attenuation factors [1/1] is equivalent to the diamond difference integration scheme. The demonstration of this proposition is done in a previous paper (Hristea and Pavelescu, 1998^[2]).

In Appendix A we present the Padé diagonal representations for the **GTMM CL** approximation. For the first three of them we observe that the sum on the row of the elements corresponding to \mathbf{T}_n^{CC} is equal to one. This leads to the similarity between the determinist cell automata and the Markov chains. In the stochastic processes we associate a transition matrix whose elements represent transition probabilities (Sinai, 1992). The **GTMM CC** transition matrix and its Padé diagonal representations are not yet stochastic matrices because the elements t_{11} and t_{22} may be negative. If we analyze the contribution of the **L** frontier to the **R** one for a square interval in S_2 approximation we notice that it has a negative value. By all means from a geometrical point of view there is not any contribution. This way the principle of integration along the neutrons is violated.

For that we consider a square spatial interval and the S_2 angular approximation. For simple geometrical reasons it results that $\gamma_n^{yx} = 1$. It is obvious that the left frontier does not contribute by transmission to the right frontier. In Figure 2 are represented the elements t_{11} for the **GTMM CC** approximation and for **GTMM CC** approximations these elements differ from 0. In fig. 2 we analyze the

dependence of the matrix element t_{11} for the **GTMM CC** and for their Padé' representations. The functional dependence refers to parameter a_{ny} measured in mean free path.

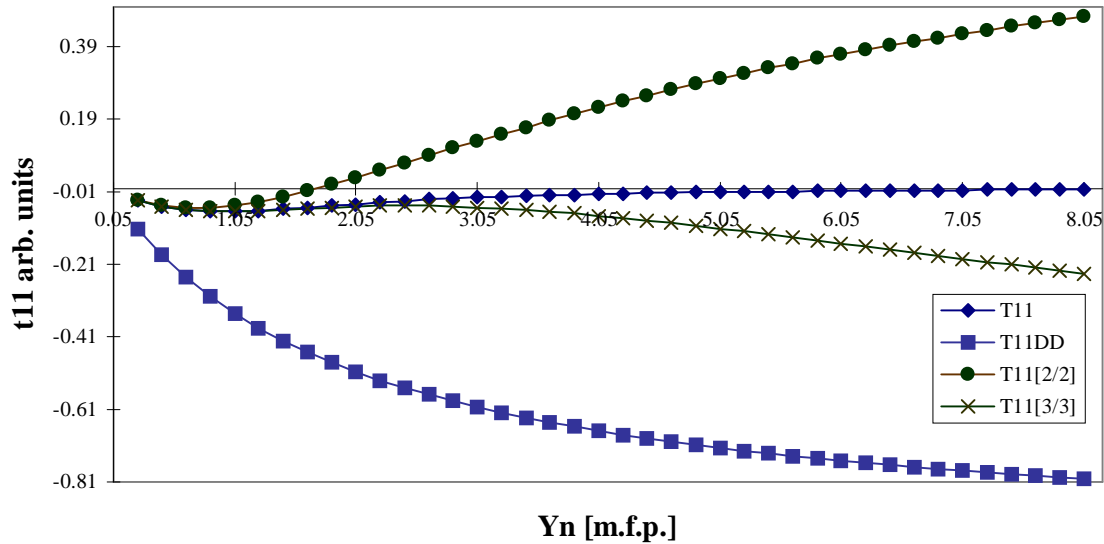


Fig. 2 The t_{11} element of the T_n matrix for the approximation **GTMM CC** and their Padé rational representations $\gamma_n^{xy} = 1$

On the basis of this observation we can conclude that neither of the approximations based on transverse integration method is inherently positively defined.

The **GTMM CC** algorithms and the **DD** scheme behave differently from a numerical point of view. There occur significant differences in the calculation of the average values of the flux. Another major difference is that of the evolution of the iterative process. There has been noticed that the **DD** scheme leads to oscillations of the iterative process and subsequently to a larger number of inner iterations. The mathematical study of these numerical phenomena is difficult due to the lack of mathematical tools for a global analysis of the transport algorithms. For slab geometry one can be demonstrated that the **GMM** algorithm in constant approximation does not lead to negative fluxes.

B) The GTMM CL approximation constant at the borders and linear within the cell- The cell automata for this approximation is:

$$\mathbf{A}_n^{\text{CL}} = (\mathbf{V}^{(5)}, \mathbf{W}^{(5)}, \mathbf{T}_n^{\text{CL}}), \left| \Psi_n^{\text{IN}} \right\rangle = \left[\psi_n^{-0}, \psi_n^{0-}, q_n^{00}, (-1)^m q_n^{10}, (-1)^l q_n^{01} \right] \quad l = \begin{cases} 0 & \text{ica} = \text{I, II} \\ 1 & \text{ica} = \text{III, IV} \end{cases}$$

$$\left| \Psi_n^{\text{OUT}} \right\rangle = \left[\psi_n^{+0}, \psi_n^{0+}, \psi_n^{00}, (-1)^m \psi_n^{10}, (-1)^l \psi_n^{01} \right] \quad m = \begin{cases} 0 & \text{ica} = \text{I, IV} \\ 1 & \text{ica} = \text{II, III} \end{cases}$$

(14)

For deriving the transition matrix we follow the procedure described in Section III A. The first step consists in finding the 0 moment of the angular flux at the outgoing transversal projection through operators: $\langle +0|$ and $\langle 0+|$. We obtain two algebraic equations.

$$\begin{aligned} \psi_n^{-0} + \gamma_n^{xy} e_{nx}^0 \psi_n^{0+} + 0\psi_n^{00} &= e^{-2a_{nx}} \psi_n^{-0} + \gamma_n^{xy} e_{nx}^0 \psi_n^{0-} + 2a_{nx} e_{nx}^0 q_n^{00} - 2a_{nx} e_{nx}^1 q_n^{10} \\ \gamma_n^{yx} e_{ny}^0 \psi_n^{-0} + \psi_n^{0+} + 0\psi_n^{00} &= 2a_{ny} e_{ny}^0 \psi_n^{-0} + e^{-2a_{ny}} \psi_n^{0-} + 2a_{ny} e_{ny}^0 q_n^{00} - 2a_{ny} e_{ny}^1 q_n^{01} \end{aligned} \quad (15)$$

To determine the moments of the angular flux within the spatial cell we apply the projection operators $\langle 00|$, $\langle 10|$ and $\langle 01|$ to the transport equation (1). We obtain the following algebraic equations which unknowns are the components of the $[\Psi^{out}]$:

$$\begin{cases} \Omega_{nx} \psi_n^{-0} + \Omega_{ny} \psi_n^{0-} + \psi_n^{00} + 0\psi_n^{10} + 0\psi_n^{01} = \Omega_{nx} \psi_n^{+0} + \Omega_{ny} \psi_n^{0+} + q_n^{00} + 0q_n^{10} + 0q_n^{01} \\ \sqrt{3}\Omega_{nx} \psi_n^{-0} + 0\psi_n^{0-} - 2\sqrt{3}\Omega_{nx} \psi_n^{00} + \psi_n^{10} + 0\psi_n^{01} = -\sqrt{3}\Omega_{nx} \psi_n^{+0} + 0\psi_n^{0+} + 0q_n^{00} + q_n^{10} + 0q_n^{01} \\ 0\psi_n^{-0} + \sqrt{3}\Omega_{ny} \psi_n^{0-} - 2\sqrt{3}\Omega_{ny} \psi_n^{00} + 0\psi_n^{10} + \psi_n^{01} = 0\psi_n^{+0} - \sqrt{3}\Omega_{ny} \psi_n^{0+} + 0q_n^{00} + 0q_n^{10} + q_n^{01} \end{cases}, \quad \begin{aligned} \Omega_{nx} &= 1/2a_{nx} \\ \Omega_{ny} &= 1/2a_{ny} \end{aligned} \quad (16)$$

In Appendix A we present the matrix equation used to obtain the transition matrix: and also the transition matrix.

The transition matrix for this approximation can be factorized so that the \mathbf{T}_n^{CC} appear in the upper left corner of the \mathbf{T}_n^{CL} . This observation helps us to analyze the Padé representation [1/1] for the elements of matrix (13).

Proposition 2 The **GTMM CL** cellular automata in the Padé' representation [1/1] of the spatial attenuation factors is equivalent to the diamond difference integration scheme $\mathbf{T}_{n[1/1]}^{\text{CL}} \equiv \mathbf{T}_n^{\text{DD}}$

Demonstration To demonstrate this proposition we compare the Pade' [1/1] (A5) with the transition matrix for the **DD** schema. It results that the Pade' representations [1/1] also coincide with the corresponding elements of the **DD** schema. The rest of the elements of transition matrix (A5) are equal to zero except the diagonal elements that are equal to one. In the circumstances of first degree moments of the guess flux equal to zero, it results that they do not contribute along the iterative process to the moment of zero degree of the flux in the spatial cell **QED**.

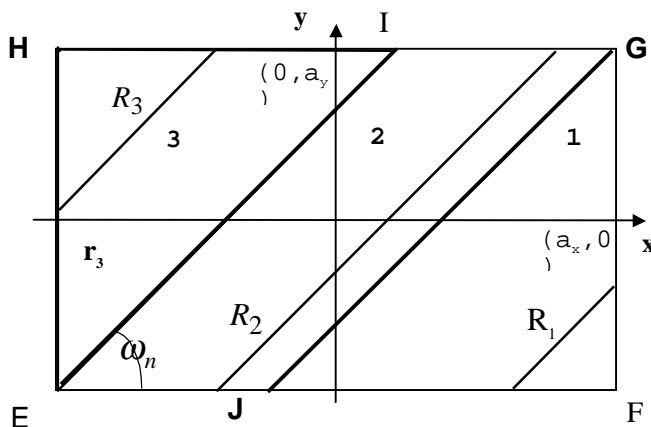
The method of transversal integration presented in this section has some particularities that occur when we build these algorithms. Not all the spatial approximations lead to distinct algorithms see the **GTMM LC** approximation.

The complexity of the formulas increases with the degree of the spatial approximation. The best example is the derivation of the **GTMM** linear - linear approximation **LL**. The algebraic system is much more complicated and implicitly the elements of the transition matrix. In this paper we shall not present this spatial approximation.

Another important observation that should be mentioned here consists in the impossibility of extending the projector method based on transversal integration to other types of geometry but Cartesian.

IV The method of projecting the S_N integral transport equation

The projector technique developed in Section III is different from that used for the discretization of the integral transport equation. Starting from the structure of the partial differential transport equation we need a method for finding out the flux at exit frontiers. This can be done by partially projecting along the two spatial directions. When using the integral form (1) of the transport S_N equation, the transversal projection is no longer necessary since we can determine in principle the angular flux at any point within the spatial cell knowing the fluxes at the incoming frontiers. In this case the principle of numerical integration along the neutrons is consequently used.



$$R_1 = a_{ny} + y_n, R_2 = 2a_{ny}, R_3 = a_{nx} + x_n$$

$$a_{ny} \rightarrow Y, a_{nx} \rightarrow X$$

$$\gamma_n^{yx} = \frac{a_{ny}}{a_{nx}} \rightarrow \Gamma, x_n = \frac{x}{\mu_n}, y_n = \frac{y}{\eta_n}$$

Fig 3 Cell's geometry for the S_N integral equation $\gamma_n^{yx} \leq 1$

VI A. Projector for integral equation - For an adequate understanding of the integral

equation for spatial projection, in Figure 3 was described the geometry specific to this method. We notice that the spatial cell is naturally split by the lines **EI** and **JG**. The unity vector of these lines coincides with the projection unity vector of the neutron' s direction. Through these lines we separate clearly the contributions of the incoming frontiers at the exit frontiers.

From this figure we notice that the spatial cell is divided naturally into three sub-domains that delimitate the influence zones of the incoming frontiers. The calculation of the moments of the angular flux within the cell is done by using either generalized balance relations or by integrating the integral transport equation on the cell surface. We used both to check the formulas for the transition elements.

We consider the spatial approximation in which the frontier fluxes are developed into Legendre polynomials up to L-1 degree and the interior fluxes up to M degree. The integral equation (3) is written considering the previous notations as:

$$\psi_n^{1(2)\bullet\bullet} = e^{-r_1(2)} \sum_{i=0}^{L-1} \psi_n^{i-} |i-\rangle + \sum_{i,j=0}^{I,J} q_n^{ij} \int_0^r dr' |ij\rangle e^{-r_1'(2)}, \quad \psi_n^{3\bullet\bullet} = e^{-r_3} \sum_{j=0}^{L-1} \psi_n^{-j} |-j\rangle + \sum_{i,j=0}^{I,J} q_n^{ij} \int_0^r dr' |ij\rangle e^{-r_3'} \quad (17)$$

We have two types of integration through which we calculate the elements of matrix T_n : the integrals at the outgoing frontiers, which are integrals defined along a line, and surface integrals.

Choosing the orthonormal basis of test function and the linearity of the projection operation of the S_N integral transport equation, we can notice that the calculation relations for the elements of the transition matrix T_n do not change alongside with the passing from a lower spatial approximation to a higher one. For the transversal projection, the complexity of the calculation formulas of the transition matrix increases with the spatial approximation.

Taking into consideration the linearity of the projection operators at the *outgoing* frontiers we evaluate the transition matrix for the **ITMM** constant-linear **CL** approximation. The elements of the transition matrix for the constant-constant **CC** approximation result simply by eliminating the elements that link the angular flux moments of higher degree.

The writing of the calculation formulas takes a lot of space, that' s why we shall simplify the notations by using: $a_{nx} \rightarrow X$, $a_{ny} \rightarrow Y$, $\gamma_n^{yx} \rightarrow \Gamma$. Due to the fact that the final formulas contain only the lengths of the real segments (not the plan projections) in fig. 3 all the notations refer to these lengths.

To simplify the integration we shall change the variables $x \rightarrow x_n, y \rightarrow y_n$. The vectors through which we represent the functions and the operators simply change into:

$$|-0\rangle \equiv |+0\rangle = 1, \langle +0| = \frac{1}{2Y} \int_{-Y}^Y dy_n, \langle 0+| = \frac{1}{2X} \int_{-X}^X dx_n, |00\rangle = 1, |10\rangle = \frac{\sqrt{3}}{X} x_n, |10\rangle = \frac{\sqrt{3}}{Y} y_n \quad (18)$$

It is necessary to simplify the equations that appear in the integral form of the transport equation (17). In these relations there appear the integrated contribution of the source along the neutron's trajectory. Since we decomposed the source into moments we can analytically calculate the integral. We determine the position (x', y') along the trajectory from the parametrical representation of the straight lines that goes through the point (x, y) , the parameter being the length r' measured in m.f.p. along the straight lines in space.

$$I = \int_0^r dr' (q^{00} + \frac{\sqrt{3}}{X} (x_n - r') q^{10} + \frac{\sqrt{3}}{Y} (y_n - r') q^{01}) e^{-r'} = q^{00} I_{00} + q^{10} I_{10} + q^{01} I_{01} \quad (19)$$

$$I_{00} = 1 - e^{-r}, I_{10} = \frac{\sqrt{3}}{X} (e^{-r} (1 + r - x_n) + x_n - 1), I_{01} = \frac{\sqrt{3}}{Y} (e^{-r} (1 + r - y_n) + y_n - 1)$$

For calculating the transfer at the outgoing frontiers it is necessary to express the fluxes at these borders depending on the sources and the incoming frontiers. While writing the formulas we shall take into account the geometrical significance and the notations in fig.3.

$$\begin{aligned} \psi_n^{1+\bullet} &= \psi_n^{0-} e^{-Y-y_n} + q_n^{00} I_{00}^1 + q_n^{10} I_{10}^1 + q_n^{01} I_{01}^1 \\ \psi_n^{2+\bullet} &= \psi_n^{0-} e^{-2Y} + q_n^{00} I_{00}^2 + q_n^{10} I_{10}^2 + q_n^{01} I_{01}^2 \\ \psi_n^{3+\bullet} &= \psi_n^{0-} e^{-X-x_n} + q_n^{00} I_{00}^3 + q_n^{10} I_{10}^3 + q_n^{01} I_{01}^3 \end{aligned} \quad (20)$$

We notice from figure 3 that at the right frontier there is a contribution only from region I. It results that $t_{11} = 0$. For the top frontier only regions 2 and 3 contribute. We have the following calculation rules with the help of projectors at the exit frontiers:

$$\langle +0|\psi_n^{+\bullet} = \langle +0|\psi_n^{1+\bullet} \quad \langle 0+|\psi_n^{2+\bullet} = \frac{1}{2X} \int_{2Y-X}^X dx_n \psi_n^{2+\bullet}, \quad \langle 0+|\psi_n^{3+\bullet} = \frac{1}{2X} \int_{-X}^{2Y-X} dx_n \psi_n^{3+\bullet}, \quad t_{11} \equiv 0, \quad (21)$$

$$t_{12} = \langle 0+|(e^{-R_3}), \quad t_{21} = \langle +0|(e^{-R_1}), \quad t_{22} = \langle 0+|(e^{-R_2}), \quad t_{1l} = \langle +0|I_{kp}^1, \quad t_{2l} = \langle 0+|(I_{kp}^2 + I_{kp}^3), \quad l = 3, 4, 5, \quad k, p = 0, 1$$

From the relations (21) we notice that the elements that make the incoming frontiers' contribution to the exit ones are positive and similarly the contribution of zero degree at the exit frontier is also positive. The first two algebraic equations are:

$$\begin{aligned} \psi_n^{+0} &= 0\psi_n^{-0} + t_{12}\psi_n^{0-} + t_{13}q_n^{00} + t_{14}q_n^{10} + t_{15}q_n^{01} \\ \psi_n^{0+} &= t_{21}\psi_n^{-0} + t_{22}\psi_n^{0-} + t_{23}q_n^{00} + t_{24}q_n^{01} + t_{25}q_n^{01} \end{aligned} \quad (22)$$

The **ITMM CL** transition matrix with their Padé [1/1] and [2/2] is presented in Appendix B.

The calculation of the elements of the **TRZ_n** matrix involves the using of double integrals. These elements are calculated with the help of projection operators applied to integral equations (17). The integration technique is exemplified for the two transition matrix elements presented here:

$$t_{31} = \frac{1}{2a_x 2a_y} \iint_{III} e^{-r} dx dy = \frac{1}{2X 2Y} \int_{-Y}^Y dy_n \int_{-X}^{Y-X+y_n} dx_n e^{-(x_n+X)} = \Gamma \frac{g_{ny}^{00}}{2Y}$$

(23)

$$t_{33} = \frac{1}{2a_x 2a_y} \left[\iint_I dx dy + \iint_{II} dx dy + \iint_{III} dx dy \right] (1 - e^{-r}) = 1 - \frac{1}{2a_x 2a_y} \iint_D dx dy e^{-r}$$

(24)

From the analysis of the elements of matrix T_n^{CL} (B2) it results that for the geometry described in Figure 3 the cellular automata associated depends on a geometrical parameter Γ and on a length Y . The parameter $\Gamma \in [0,1]$ does not present a major problem because it does not appear in formulas at the denominator. The Y parameter by all means can be equal to zero in case of a cell without any material (void). For the implementation in a programming language when $\Sigma_t \rightarrow 0$, the use of the exponential function from the library of the language leads to numerical indeterminacies of 0/0 type. The corresponding approximation of the automata in this case represents a problem that is dealt in the next section and in Appendix B.

The case in which $\gamma_n^{yx} > 1 \Leftrightarrow \gamma_n^{xy} < 1$ shall be treated separately following the same calculation steps. For this the cellular automata depends on the γ_n^{xy} parameter and on the distance X . There can be avoided such a laborious calculation by exchanging the axes x and y . Thus we can use the elements of the transition matrix calculated for $\gamma_n^{yx} \leq 1$, by replacing the parameter Γ with γ_n^{xy} and the distance Y with distance X .

IV B Qualitative analysis of ITMM CL approximation -The qualitative analysis of **ITMM** algorithms consists in deriving the main features of these algorithms starting from the analysis of the structure of transition elements of the matrix. The adequate representation of these constants of structure is necessary in the case of the void. The use of the exponential function from the library of the

programming language leads to indeterminations of 0/0 type. The representation of the elements of the transition matrix is necessary for the algorithm not to lead to such indeterminations.

Like **GTMM** algorithms, we use the development of the spatial attenuation factors in rational Pade' fractions for **ITMM** approximations also. In this case we can derive as well as for slab geometry (Hristea and Pavelescu, 1998^[1]) the elements of the transition matrix in vacuum. For this we use the integral equation of vacuum transfer and apply the projector method for deriving the elements of this \mathbf{T}_n matrix. In vacuum the distances are measured in cm and the sources in $n/\text{cm}^3\text{s}$.

We introduce the following notations: $a'_{nx} \rightarrow X'$, $a'_{ny} \rightarrow Y'$, $\gamma_n^{yx} \rightarrow \Gamma X'$, $Y'[\text{cm}]$. The integral equations for the three regions represented in Figure 3 are:

$$\begin{aligned} \psi_n^{1(2)\bullet\bullet} &= \psi_n^{0-} + I_{00}^{1(2)} Q^{00} + I_{10}^{1(2)} Q^{10} + I_{01}^{1(I2)} Q^{01}, & I_{00}^{1(2)} &= Y' + y'_n, & I_{01}^{1(2)} &= \frac{\sqrt{3}}{2Y'} (Y' + y'_n)(y'_n - Y') \\ & & I_{10}^{1(2)} &= \frac{\sqrt{3}}{2X'} (Y' + y'_n)(2x'_n - Y' - y'_n) & & \\ \psi_n^{3\bullet\bullet} &= \psi_n^{-0} + I_{00}^3 Q^{00} + I_{10}^3 Q^{10} + I_{01}^3 Q^{01}, & I_{00}^3 &= X' + x'_n, & I_{10}^3 &= \frac{\sqrt{3}}{2Y'} (X' + x'_n)(x'_n - X') \\ & & I_{01}^3 &= \frac{\sqrt{3}}{2Y'} (X' + x'_n)(2y'_n - X' - x'_n) & & \end{aligned} \quad (25)$$

The \mathbf{T}_n matrix in vacuum is obtained following the same procedure as well as for the situation in which the total section is different from 0.

$$\mathbf{T}_{\text{void}}^{CL} = \begin{bmatrix} 0 & 1 & Y' & \frac{\sqrt{3}Y'(3-2\Gamma)}{3} & \frac{-\sqrt{3}Y'}{3} \\ \Gamma & 1-\Gamma & Y'(2-\Gamma) & \frac{-\sqrt{3}\Gamma Y'(3-2\Gamma)}{3} & \frac{\sqrt{3}\Gamma Y'}{3} \\ \frac{\Gamma}{2} & \frac{2-\Gamma}{2} & \frac{Y'(3-\Gamma)}{3} & \frac{-\sqrt{3}\Gamma Y'(2-\Gamma)}{6} & \frac{-\sqrt{3}Y'(2-\Gamma)}{6} \\ -\frac{\sqrt{3}\Gamma(3-2\Gamma)}{6} & \frac{\sqrt{3}\Gamma(3-2\Gamma)}{6} & \frac{\sqrt{3}\Gamma Y'(2-\Gamma)}{6} & \frac{Y'(5-5\Gamma+\Gamma^3)}{5} & \frac{-\Gamma Y'(5-3\Gamma)}{5} \\ \frac{\sqrt{3}\Gamma}{6} & \frac{-\sqrt{3}\Gamma}{6} & \frac{\sqrt{3}Y'(2-\Gamma)}{6} & \frac{-\Gamma Y'(5-3\Gamma)}{10} & \frac{Y\Gamma}{5} \end{bmatrix} \quad (26)$$

The choosing of the Pade' approximation order is a difficult task. For making correct comparisons we consider that the total section is a small infinite of order 1 and the scattering ratio is a number different from 0. We develop the elements of the (B2) matrix retaining only the first approximation.

In the Appendix B are represented the transition matrix for the development of the spatial attenuation factor in Padé fractions: [1/1] and [2/2]. By comparing these approximations to the elements of the matrix (24) we notice that for the Pade' approximations [1/1] and [2/2] the vacuum deviation

becomes significant. Diagonal Padé approximations superior to order 2 well approximate the elements of the transition matrix.

An important property arise for the **ITMM CC** approximation:

$$\mathbf{T}_n^{CC} = \begin{bmatrix} 0 & e_{ny}^0 & g_{ny}^{00} \\ \Gamma e_{ny}^0 & e^{-2Y}(1-\Gamma) & \Gamma g_{ny}^{00} + 2Ye_{ny}^0(1-\Gamma) \\ \frac{\Gamma g_{ny}^{00}}{2Y} & \frac{\Gamma g_{ny}^{00}}{2Y} + e_{ny}^0(1-\Gamma) & \Gamma(1 - \frac{g_{ny}^{00}}{Y}) + g_{ny}^{00}(1-\Gamma) \end{bmatrix}, \quad \begin{aligned} e_{ny}^0 + g_{ny}^{00} &= 1 \\ \Gamma e_{ny}^0 + e^{-2Y}(1-\Gamma) + \Gamma g_{ny}^{00} + 2Ye_{ny}^0(1-\Gamma) &= 1 \\ \frac{\Gamma g_{ny}^{00}}{2Y} + \frac{\Gamma g_{ny}^{00}}{2Y} + e_{ny}^0(1-\Gamma) + \Gamma(1 - \frac{g_{ny}^{00}}{Y}) + g_{ny}^{00}(1-\Gamma) &= 1 \end{aligned} \quad (27)$$

Proposition 3 The **ITMM CC** transition matrix is stochastic

Demonstration The demonstration of this proposition goes back to the demonstration of the positiveness of the transition matrix (27). This comes directly from that the elements of the matrix are obtained by linear or surface integration of some positive functions. **QED**

V Calculations and Results

Numerical tests presented next create a chart of main properties of the algorithms described within this paper. We are interested in the dependence of the numerical integration precision on the discretization of the problem. We use benchmark tests very well corroborated (Khalil 1986, Warin 1994), which point out the behaviour within limit areas of the programs based on projector method. The tests contain both problems with weak and strong scattering materials. We compare the performances of **ITMM** and **GTMM** and of this Padé representations algorithms depending on the dimension of the spatial interval. We shall further on use the maximum optical way D_{opt} , which represents the maximum of mediate optical ray on all angular directions corresponding to the S_N approximation.

$$D_{opt} = \max_{J \in N_{region}} \bar{r}_J, \quad \bar{r}_J = \sum_{n=1}^{N(N+2)/8} w_n \bar{r}_n, \quad \bar{r}_n = \langle 00 | r_n = \frac{U}{3}(3-\Gamma), \quad U = \begin{cases} Y & \text{daca } \Gamma \equiv \gamma_n^{yx} \leq 1 \\ X & \text{daca } \Gamma \equiv \gamma_n^{xy} < 1 \end{cases} \quad (28)$$

Because all the benchmark cases treated here report the averaged flux on the material we plot the dependence of averaged relative error on the D_{opt} .

$$E_{med} = \frac{\sum_{j \in N_{region}} V_j \varepsilon_j}{V_T}, \quad V_T = \sum_{j \in N_{region}} V_j, \quad \varepsilon_j = \frac{|\bar{\Phi}_j^{rep} - \bar{\Phi}_j^{calc}|}{\bar{\Phi}_j^{rep}} \quad (29)$$

where V_j is the volume of the material region.

VA Benchmark problem containing nearly voided region - The benchmark case treated in this paragraph consists in a problem containing a nearly voided region (Khalil, 1985). The geometry and material properties are shown in Figure 4 and Table 1.

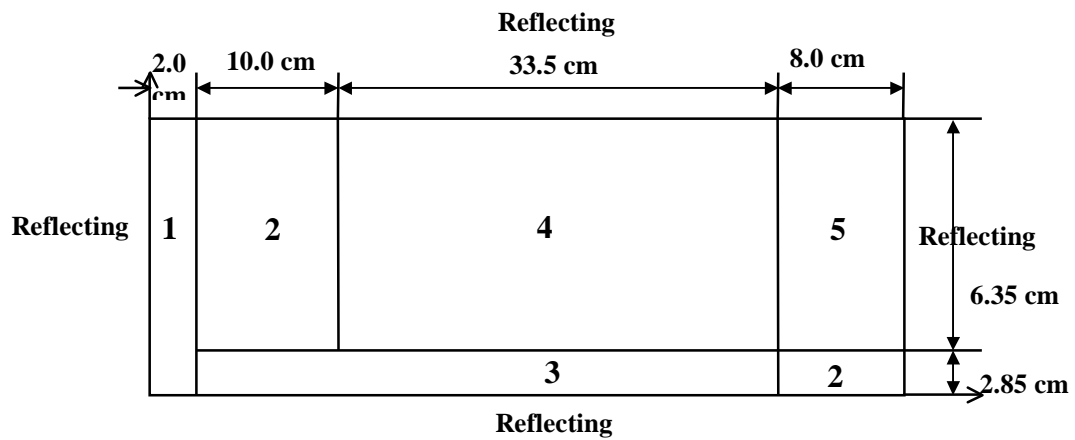


Fig. 4 The geometry for a problem containing a nearly voided region

Table 1 Material properties for the nearly voided problem

Material No.	Source ($\text{cm}^{-3}\text{s}^{-1}$)	Σ_a (cm^{-1})	Σ_s (cm^{-1})	Σ_t (cm^{-1})
1	0	0.4	0.00	0.4
2	0	0.027	0.073	0.1
3	0	0.00203	0.00497	0.007
4	0.29	0.0162	0.0738	0.09
5	0.07	0.0162	0.0738	0.09

The purpose of these tests is to compare integration precision for the two classes of algorithms presented in the paper. A special attention will be paid to the evaluation of the integration for extremely thin intervals. The evolution of the integration precision through mesh refining imposes the representation through rational fractions of the transition matrixes elements. The choosing of an adequate representation is a problem that involves an empiric study on specific cases and through different Padé approximations mentioned in Appendices A and B. As it is difficult to estimate the overall precision for the numerical integration of the transport equation, we present numerical experiments that can offer an empiric limit of the transport algorithms' performances developed in this paper.

Table 2 The material averaged fluxes for a benchmark problem containing a nearly voided region

Algorithm	Zone 1	Zone 2	Zone 3	Zone 4	Zone 5
TICC	0.15592E+01	0.48814E+01	0.79685E+01	0.98062E+01	0.79900E+01

TGCC	0.15014E+01	0.49673E+01	0.80725E+01	0.98353E+01	0.81130E+01
TICL	0.15461E+01	0.48629E+01	0.79777E+01	0.98471E+01	0.79856E+01
TGCL	0.14734E+01	0.49080E+01	0.81106E+01	0.99392E+01	0.80832E+01
TWODANT'	0.14734E+01	0.49107E+01	0.81133E+01	0.99431E+01	0.80834E+01

(Khalil, 1985)

The data obtained through the programs described above are compared with the results obtained through the **TWODANT** code for mesh 10x3 in S_8 approximation (Khalil, 1985). In Table 2 we present the average flux by composition for S_N angular approximation obtained through **ITMM CC** (**TICC**), **GTMM CC** (**TGCC**), **ITMM CL** (**TICL**) and **GTMM CL** (**TGCL**) approximations.

We notice that the best results are obtained through the **TGCL** algorithm. The approximations based on integral equation projection significantly differ from the results obtained through the **TWODANT** code (Khalil, 1985).

The purpose of this test is the approach of the evolution for the precision of the numerical results on refining spatial intervals. By increasing the number of spatial intervals we notice that both **TGCL** and **TICL** algorithms leads to numerical instabilities. In Figure 5a we present the evolution of the maximum relative error for **TICC** algorithm and with the algorithms obtained through diagonal rational Pade' fractions. There are tested [1/1] (**TIP1CC**), [2/2]

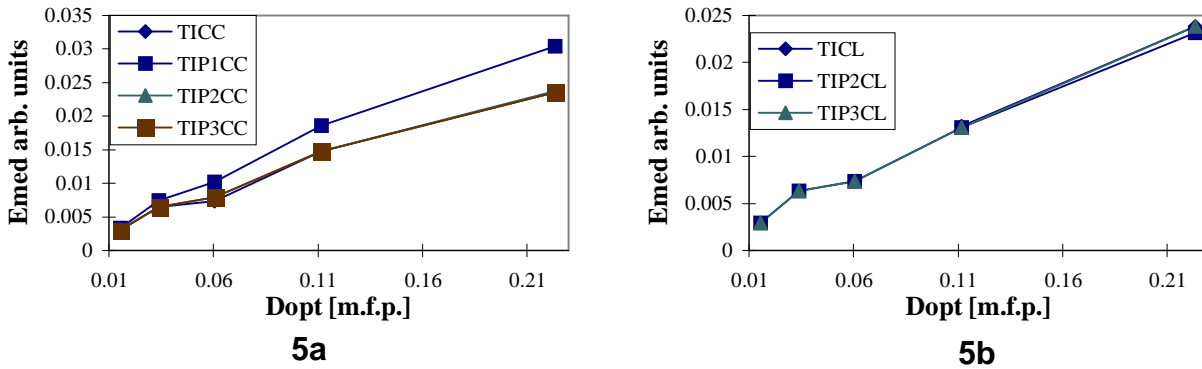


Figure 5 The averaged relative error for ITMM algorithms and their diagonal Pade' approximations

From Figure 5a we observe that the **TIP1CC** algorithm is less accurate than the other representations of the **TICC** algorithm. In Figure 5b we plot the averaged relative errors obtained with **ITMM CL** (**TICL**) and their Padé diagonal representation [2/2] (**TIP2CL**) and [3/3] (**TIP3CL**). On this value field, Pade' representations [2/2] and [3/3] lead to identical results for constantlinear spatial

approximation. We notice that **TICL** fail to converge for D_{opt} less than 0.11 m.f.p. These results for Padé representations should be studied for larger intervals also, so that we can establish a domain for their applicability.

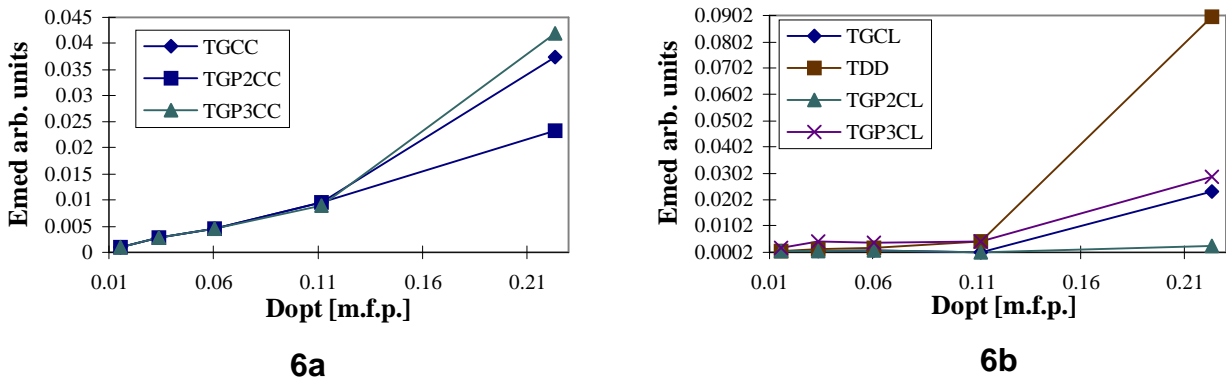


Figure 6 The averaged relative error for GTMM algorithms and their diagonal Padé' approximations

In Figure 6a we present the averaged relative errors obtained with **GTMM CC (TGCC)** and their Padé' approximations [2/2] (**TGP2CC**) and [3/3] (**TGP3CC**). In Figure 6b we represent also the averaged relative errors obtained with **GTMM CL (TGCL)** and their Padé representations. For this spatial approximation we show the results obtained with diamond difference schema which are obtained as Padé' [1/1] representation of the **GTMM CL** (see proposition 3). **GTMM CL** schema fails to converge for D_{opt} less then 0.0234 m.f.p. From the figure 6b we see that **TGP3CL** is less good than **TGP2CL** ones and than **TGCL** also. This is not the case for the **CC** approximation (see Figure 6a). For D_{opt} greater than 0.11 m.f.p. the diamond difference schema is less accurate than all other algorithms presented.

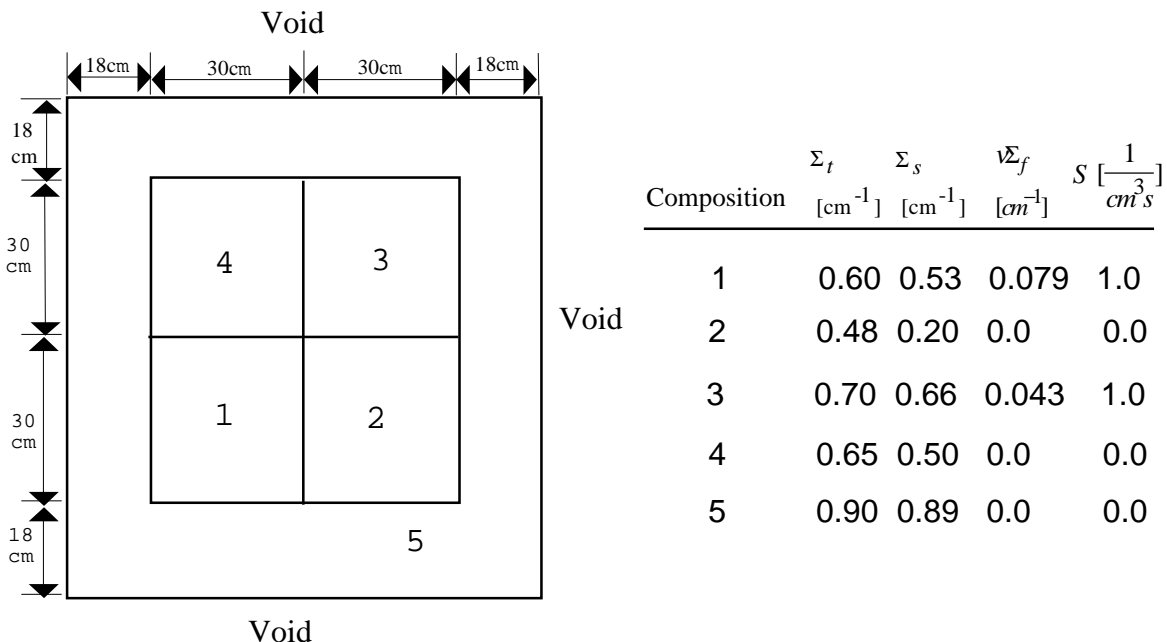


Fig. 7 Geometry and material composition for the Stepanek test problem

VB The Stepanek test problem- The problem presented in Figure 7 (Khalil, 1985) and (Warin and Vaudeschal 1995) presents both a fixed source and an eigenvalue benchmark test. We present this problem for continuing the analysis of Pade' representations behavior for situations when the length of the intervals is greater than 0.25 m.f.p.

Table 3 The average flux by composition for the Stepanek fixed sources problem

Algorithm	Zone 1	Zone 2	Zone 3	Zone 4	Zone 5	E_{med}
TICC	11.817	0.56628	18.808	0.88377	1.6104	4.7980 -02
TICL	11.881	0.55480	18.988	0.86259	1.5712	2.6065 -02
TGCC	11.870	0.55600	18.948	0.86441	1.5838	3.1971 -02
TGCL	11.961	0.53936	19.205	0.83307	1.5257	3.9743 -04
TDD	11.960	0.53969	19.202	0.83364	1.5267	1.1641 -04
TWODANT	11.960	0.53968	19.202	0.83364	1.5263	

(Khalil, 1985)

In Table 3 we present the average flux by composition for a spatial grid with 100x100 mesh cells and for S_8 approximation (Khalil, 1985). The algorithms **TGCL** and **TDD** lead to closest results in good concordance with the **TWODANT**. The **TICL** algorithm is not so accurate as we expect. This result needs a supplementary analysis.

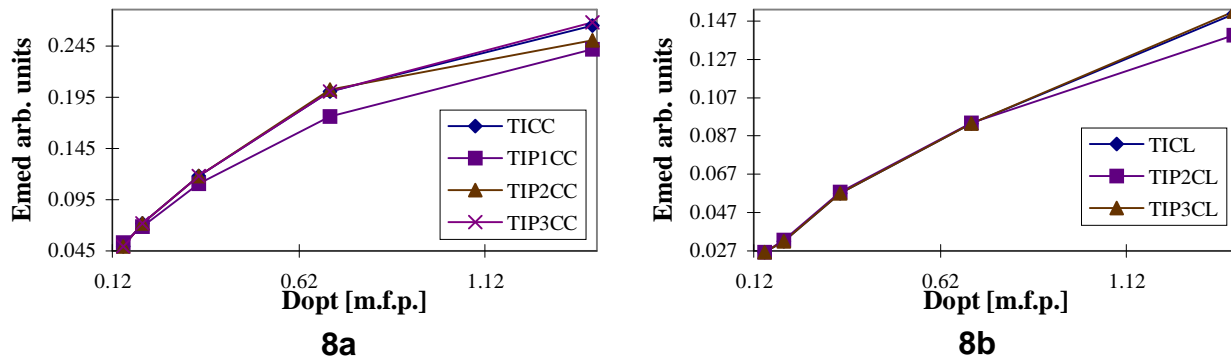


Figure 8 The averaged relative error for Stepanek test problem - ITMM algorithms and their diagonal Pade' approximations

In Figure 8 we present comparatively the evolution of the integrating precision in S_4 angular approximation obtained with **ITMM** and **GTMM** algorithms. For both spatial approximations the Pade' [3/3] representation leads to identical results as analytic approximations. The study of Pade' approximations in the domain of larger optical paths for **ITMM CL** algorithm is described in fig. 8b. At the side are tested **ITMM CL** algorithm and Pade' representations [2/2] (**TIP2CL**) and [3/3] (**TIP3CL**).

For this spatial approximation Padé' representation [2/2] leads to better results than "exact" representation for larger intervals. Padé' approximation [3/3] leads to predictable results for thin intervals with D_{opt} smaller than 0.2 m.f.p. There can be reached a total concordance with "exact" approximation.

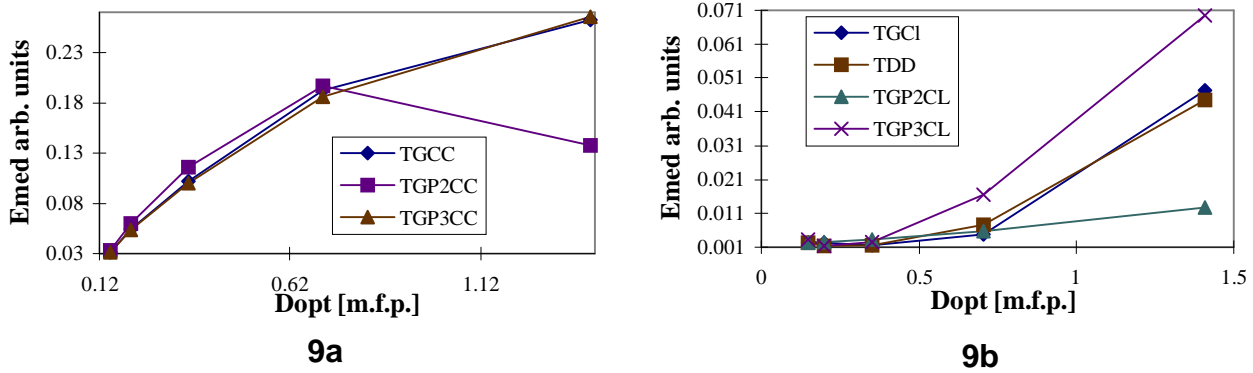


Figure 9 The averaged relative error for Stepanek test problem - GTMM algorithms and their diagonal Padé' approximations

In Figure 9a we continue the approach of Padé approximations for **GTMM CC** algorithm. Padé' representation [2/2] (**TGP2CC**) in the area of large intervals leads to a superior precision to GTMM CC algorithm. But we notice at the same time that for smaller spatial intervals the precision of **TGP2CC** algorithm is weaker than that of **TGP2CC** algorithm. Interesting results are obtained analyzing the fig. 9b. The **TGP2CL** algorithm leads to better results than: **TGCL**, **TDD** and **TGP3CL** algorithms. From this it results that **TGP2CL** algorithm may be used not only for thin spatial intervals.

Table 4 The multiplication factor for the Stepanek test problem

Spatial grid	TICC	TICL	TGCC	TGCL	TDD	TGP2CL	TGP3CL
24x22	0.92680	0.98870	0.93171	1.0095	1.0076	1.01032	1.00636
50x50	0.96612	0.99354	0.97147	1.0094	1.0088	1.00962	1.00788
68x68	0.98699	0.99873	0.99330	1.0092	1.0089	1.00924	1.00915

The results for the k_{eff} Stepanek test problem are summarized in Table 4. A good approximation for the multiplication factor is obtained with **TGCL** and with the diamond difference schema **TDD**. From this we can conclude that the **GTMM CL** approximation is competitive with the diamond difference schema.

VI Conclusions on the projector method

The solving algorithms for the transport equation based on the projector method presented so far represent only a part of the calculation algorithms we have obtained. The method of presenting the algorithms differs from the usual presentation by the fact that for the analysis of the numerical performances it is necessary to present the algorithms explicitly. The writing of the numerical integration through a single \mathbf{T}_n matrix within the cell in the phase space simplifies the comparison of the algorithms. If we also take into account that the numerical integration of the S_N transport equation is an iterative process for which we start with a guess flux, then a few interesting propositions results by which some numerical approximations prove to be useless (Hristea, 1999).

The numerical tests next presented point out the fact that the **GTMM** schemes are far more precise for the determination of the average values within the material areas. By all means, from the facts not presented here it results that the transversal integration method shows some deficiencies that occur for the determination of the fine flux distributions. One of the most important results of this paper consists in rational representations of algorithms based on projector method.

A The GTMM CL transition matrix calculus and its Padé representation

The transition matrix for the **GTMM CL** results by solving the matrix equation $\mathbf{A}_n^{\text{CL}}[\Psi_n^{\text{out}}] = \mathbf{B}_n^{\text{CL}}[\Psi_n^{\text{in}}]$

(see (16) and (17)). The matrix \mathbf{A}_n^{CL} and \mathbf{B}_n^{CL} are:

$$\mathbf{A}_n^{\text{CL}} = \begin{bmatrix} 1 & \gamma_n^{xy} e_{nx}^0 & 0 & 0 & 0 \\ \gamma_n^{yx} e_{ny}^0 & 1 & 0 & 0 & 0 \\ \Omega_{nx} & \Omega_{ny} & 1 & 0 & 0 \\ \sqrt{3}\Omega_{nx} & 0 & -2\sqrt{3}\Omega_{nx} & 1 & 0 \\ 0 & \sqrt{3}\Omega_{ny} & -2\sqrt{3}\Omega_{ny} & 0 & 1 \end{bmatrix}, \mathbf{B}_n^{\text{CL}} = \begin{bmatrix} e^{-2a_{xn}} & \gamma_n^{xy} e_{nx}^0 & 2a_{nx}e_{nx}^0 & -2a_{nx}e_{nx}^0 & 0 \\ \gamma_n^{yx} e_{ny}^0 & e^{-2a_{yn}} & 2a_{ny}e_{ny}^0 & 0 & -2a_{ny}e_{ny}^1 \\ \Omega_{nx} & \Omega_{ny} & 1 & 0 & 0 \\ -\sqrt{3}\Omega_{nx} & 0 & 0 & 1 & 0 \\ 0 & -\sqrt{3}\Omega_{ny} & 0 & 0 & 1 \end{bmatrix} \quad (\text{A1})$$

The transition matrix is:

$$\mathbf{T}_n^{\text{CL}} = \frac{1}{\Delta_n} \begin{bmatrix} e^{-2a_{nx}} - e_{nx}^0 e_{ny}^0 & 2a_{nx}e_{nx}^0 e_{ny}^0 & 2a_{nx}e_{nx}^0 g_{ny}^{00} & -2a_{nx}e_{nx}^1 & 2a_{nx}e_{nx}^0 e_{ny}^1 \\ 2a_{ny}e_{nx}^0 e_{ny}^0 & e^{-2a_{ny}} - e_{nx}^0 e_{ny}^0 & 2a_{ny}e_{ny}^0 g_{nx}^{00} & 2a_{ny}e_{ny}^0 e_{nx}^1 & -2a_{ny}e_{ny}^1 \\ e_{nx}^0 g_{ny}^{00} & e_{ny}^0 g_{nx}^{00} & g_{nx}^{00} g_{ny}^{00} & e_{nx}^1 g_{ny}^{00} & e_{ny}^1 g_{nx}^{00} \\ e_{nx}^1 & -e_{ny}^1 e_{nx}^1 & -e_{nx}^1 g_{ny}^{00} & h_{nxy}^{11} & -e_{nx}^1 e_{ny}^1 \\ -e_{nx}^0 e_{ny}^1 & e_{ny}^1 & -e_{ny}^1 g_{nx}^{00} & -e_{nx}^1 e_{ny}^1 & h_{nyx}^{11} \end{bmatrix}, \mathbf{T}_n^{\text{CL}} = \begin{bmatrix} \mathbf{T}_n^{\text{CC}} & \mathbf{H}_{12} \\ \mathbf{H}_{21} & \mathbf{H}_{22} \end{bmatrix} \quad (\text{A2})$$

$$\Delta_n = 1 - e_{nx}^0 e_{ny}^0, h_{nuv}^{11} = (e_{nu}^1)^2 e_{nv}^0 + g_{nu}^{11} \Delta_n, g_{nu}^{11} = 1 + \sqrt{3} e_{nu}^1 \frac{1 + a_{nu}}{a_{nu}}, u, v = x, y$$

The $\mathbf{T}_{n[1/1]}^{CL}$, $\mathbf{T}_{n[2/2]}^{CL}$ and $\mathbf{T}_{n[3/3]}^{CL}$ matrices are obtained using the Pade' representation for the

$\exp(-2y)$ spatial attenuation factor of order [1/1], [2/2] and [3/3] (Baker jr. and Graves-Morris. 1981).

$$e_{[1/1]}^{-2Y} = \frac{P_1(-Y)}{P_1(Y)}, e_{[2/2]}^{-2Y} = \frac{P_2(-Y)}{P_2(Y)}, e_{[3/3]}^{-2Y} = \frac{P_3(-Y)}{P_3(Y)}, \quad (A3)$$

$$P_1(Y) = 1 + Y, P_2(Y) = 3 + 3Y + Y^2, P_3(Y) = 15 + 15Y + 6Y^2 + Y^3$$

We obtain:

$$\mathbf{T}_{n[1/1]}^{CL} = \frac{1}{D} \begin{bmatrix} D - 2(1+Y) & 2 & 2Y & 0 & 0 \\ 2\gamma_n^{yx} & D - 2\gamma_n^{yx}(1+X) & 2Y & 0 & 0 \\ \gamma_n^{yx} & 1 & Y & 0 & 0 \\ 0 & 0 & 0 & D & 0 \\ 0 & 0 & 0 & 0 & D \end{bmatrix} D = 1 + Y + \gamma_n^{yx} \quad (A4)$$

$$\mathbf{T}_{n[2/2]}^{CL} = \frac{1}{D} \begin{bmatrix} D - 6P_2(Y) & 18 & 6YB_1 & 2\sqrt{3}XP_2(Y) & -6\sqrt{3}Y \\ 18\gamma_n^{yx} & D - 6\gamma_n^{yx}P_2(X) & 6YA_1 & -6\sqrt{3}Y & 2\sqrt{3}\gamma_n^{yx}YP_2(X) \\ 3\gamma_n^{yx}B_1 & 3A_1 & YA_1B_1 & -\sqrt{3}YB_1 & -\sqrt{3}YA_1 \\ -\sqrt{3}P_2(Y) & 3\sqrt{3} & \sqrt{3}YB_1 & D - 3(P_2(Y) + \gamma_n^{yx}B_1) & -3Y \\ 3\sqrt{3}\gamma_n^{yx} & -\sqrt{3}\gamma_n^{yx}P_2(X) & \sqrt{3}YA_1 & -3Y & D - 3(\gamma_n^{yx}P_2(X) + A_1) \end{bmatrix} \quad (A5)$$

$$D = P_2(X)\gamma_n^{yx}B_1 + 3A_1, A_1 = x + 3, B_1 = y + 3$$

$$\mathbf{T}_{n[3/3]}^{CL} = \frac{1}{D} \begin{bmatrix} D - 2A_2P_3(Y) & 2A_2B_2 & 2YA_2B_3 & 10\sqrt{3}XP_3(Y) & -10\sqrt{3}YA_2 \\ 2\gamma_n^{yx}A_2B_2 & D - 2\gamma_n^{yx}P_3(X)B_2 & 2YA_3B_2 & -10\sqrt{3}YB_2 & 10\sqrt{3}\gamma_n^{yx}YP_3(X) \\ \gamma_n^{yx}A_2B_3 & A_3B_2 & YA_3B_3 & -5\sqrt{3}YB_3 & -5\sqrt{3}YA_3 \\ -5\sqrt{3}P_3(Y) & 5\sqrt{3}B_2 & 5\sqrt{3}YB_3 & D - 15(\gamma_n^{yx}B_3 + P_3(Y)) & -75Y \\ 5\sqrt{3}\gamma_n^{yx}A_2 & -5\sqrt{3}\gamma_n^{yx}P_3(X) & 5\sqrt{3}YA_3 & -75Y & D - 15(A_3 + \gamma_n^{yx}P_3(X)) \end{bmatrix} \quad (A6)$$

$$D = \gamma_n^{yx}(P_3(X)B_2 + (75 + 90X + 35X^2 + 6X^3)Y) + 15A_3, A_2 = 15 + X^2, A_3 = 15 + 5X + X^2,$$

$$B_2 = 15 + Y^2, B_3 = 15 + 5Y + Y^2$$

Each element of the matrix (A5-A7) is written so that it should not lead to 0/0 indetermination if

$\Sigma_t \rightarrow 0$. The elements t_{ij} , $i \leq 3, j \leq 3$ are the same as for the T_n^{CC} matrix. The Pade' representation

preserves the property that: $\sum_{j=1}^3 t_{ij[m/m]} = 1, i = 1, 2, 3$.

B The ITMM CL approximation and their diagonal Pade' [1/1] and [2/2] representation

The transition matrix for the **ITMM CL** spatial approximation results using the matrix:

$$\mathbf{A}_n^{\text{CL}} = \begin{bmatrix} 1 & 0 & 0 & 0 & 0 \\ 0 & 1 & 0 & 0 & 0 \\ \Omega_{nx} & \Omega_{ny} & 1 & 0 & 0 \\ \sqrt{3}\Omega_{nx} & 0 & -2\sqrt{3}\Omega_{nx} & 1 & 0 \\ 0 & \sqrt{3}\Omega_{ny} & -2\sqrt{3}\Omega_{ny} & 0 & 1 \end{bmatrix}, \mathbf{B}_n^{\text{CL}} = \begin{bmatrix} 0 & t_{12} & t_{13} & t_{14} & t_{15} \\ t_{21} & t_{22} & t_{23} & t_{24} & t_{25} \\ \Omega_{nx} & \Omega_{ny} & 1 & 0 & 0 \\ -\sqrt{3}\Omega_{nx} & 0 & 0 & 1 & 0 \\ 0 & -\sqrt{3}\Omega_{ny} & 0 & 0 & 1 \end{bmatrix}$$

(B1)

where the elements that appear in the matrix \mathbf{B}_n^{CL} are calculated with the relations (22). The transition matrix is:

$$\mathbf{T}_n^{\text{CL}} = \begin{bmatrix} 0 & e_{ny}^0 & g_{ny}^{00} & \frac{\sqrt{3}(e^{-2Y}B1+B2)}{2Y^2} & e_{ny}^1 \\ e_{ny}^0\Gamma & e^{-2Y}(1-\Gamma) & \frac{e^{-2Y}B3+Y-\Gamma}{2Y} & \frac{-\sqrt{3}\Gamma(e^{-2Y}B4+B5)}{2Y^2} & \frac{-\sqrt{3}(e^{-2Y}B6+B7)}{2Y^2} \\ \frac{\Gamma g_{ny}^{00}}{2Y} & \frac{e^{-2Y}B8+2Y-\Gamma}{4Y^2} & \frac{e^{-2Y}B9+B10}{2Y^2} & \frac{\sqrt{3}\Gamma(e^{-2Y}B11+B12)}{4Y^3} & \frac{\sqrt{3}(e^{-2Y}B13+B14)}{4Y^3} \\ \frac{-\sqrt{3}\Gamma(e^{-2Y}B15+B16)}{4Y^3} & \frac{\sqrt{3}\Gamma(e^{-2Y}B17+Y-\Gamma)}{4Y^3} & -t_{10}^{00} & \frac{e^{-2Y}B18+B19}{2Y^4} & \frac{3\Gamma(e^{-2Y}B20+B21)}{4Y^4} \\ \frac{-\Gamma e_{ny}^1}{2Y} & \frac{\sqrt{3}(e^{-2Y}B22+B23)}{4Y^3} & \frac{t_{10}^{10}}{\Gamma} & t_{01}^{10} & \frac{e^{-2Y}B24+B25}{2Y^4} \end{bmatrix} \quad (\text{B2})$$

where:

$$\begin{aligned} B1 &= Y - 2\Gamma(1+Y), B2 = 2Y^2 - Y + 2\Gamma(1-Y), B3 = \Gamma - 2Y(1-\Gamma), B4 = 2Y\Gamma(1+Y) - Y - 2Y^2, B5 = Y - \Gamma, \\ B6 &= 2G + 3YG - 2Y + 2Y^2(G-1), B7 = GY - 2G + 2Y(1-Y), B8 = 2Y(\Gamma-1) + \Gamma, B9 = Y - \Gamma(1+Y), B10 = 2Y^2 - Y + \Gamma(1-Y), \\ B11 &= 2Y^2(\Gamma-1) + 2Y(2\Gamma-1) + 3\Gamma, B12 = 2Y((1+\Gamma) - 2Y^2 - 3\Gamma), B13 = 3\Gamma + 4Y\Gamma - 2Y + 2Y^2(\Gamma-1), B14 = 2Y(1+\Gamma) - 3\Gamma - \\ &- 2Y^2, B15 = Y - 2\Gamma(1+Y), B16 = 2\Gamma - Y + 2Y(Y-\Gamma), B17 = \Gamma + Y(2\Gamma-1) + 2Y^2(\Gamma-1), B18 = \Gamma^3(6 + 2Y^3 + 6Y^2 + 9Y) - \\ &- 3Y^2\Gamma(Y+1) + Y^3, B19 = 3\Gamma^3(Y-2) - 3Y^2\Gamma(Y-1) - Y^3 + 2Y^4, B20 = \Gamma(6 + 9Y + 6Y^2 + 2Y^3), B21 = Y(3 - 2Y) + 3G(Y-2), \\ B22 &= \Gamma(2 + 3Y + 2Y^2) - 2Y((1+Y)), B23 = 2Y(1-Y) + \Gamma(Y-2), B24 = 3\Gamma(2 + 4Y + 3Y^2 + Y^3) - 3Y(1 + 2Y + Y^2), \\ B25 &= \Gamma(3Y^2 - Y^3 - 6) + Y(3 + 2Y^3 - 3Y^2) \end{aligned} \quad (\text{B3})$$

The Padé approximation [1/1] is insufficient for evaluating the elements of the two matrices that link moments of order 1. A simple calculus demonstrates this. By all means, for the **ITMM CC** approximation this representation is interesting numerically. The elements of the transfer and transition matrixes for the Padé approximation are:

$$\mathbf{T}_{n[1/1]}^{\text{CC}} = \frac{1}{1+Y} \begin{bmatrix} 0 & 1 & Y \\ \Gamma & (1-Y)(1-\Gamma) & Y(2-\Gamma) \\ \Gamma/2 & (2-\Gamma)/2 & Y \end{bmatrix}$$

(B4)

We notice that the summing of the row elements for this matrix is equal to unity. A higher approximation to the previous ones is the Padé approximation [2/2]. We shall next present the transition matrix:

$$\mathbf{T}_{n[2/2]}^{\text{CL}} = \frac{1}{P_2(Y)} \begin{bmatrix} 0 & 3 & Y(3+Y) & Ya_{14} & -\sqrt{3}Y \\ 3\Gamma & (1-\Gamma)P_2(-Y) & Y(6-3\Gamma+Y\Gamma) & -Ya_{24} & a_{25} \\ \Gamma(3+Y) & 6+\Gamma(Y-3) & 2Y(3-\Gamma+Y) & -\Gamma a_{34} & -a_{34} \\ -\Gamma a_{14} & \Gamma a_{24} & \Gamma a_{34} & a_{44} & 3\Gamma Y(1-\Gamma) \\ \sqrt{3}\Gamma & -\sqrt{3}(\Gamma+2Y-Y\Gamma) & a_{34} & 3\Gamma Y(1-\Gamma) & Y(Y+\Gamma) \end{bmatrix}$$

(B5)

$$a_{14} = \sqrt{3}(3-2\Gamma+Y), \quad a_{24} = \sqrt{3}\Gamma Y(3-2\Gamma+Y\Gamma-Y), \quad a_{25} = \sqrt{3}Y(\Gamma+2Y-\Gamma Y), \quad a_{34} = \sqrt{3}Y(2-\Gamma) \\ a_{44} = 2Y(3+Y+\Gamma^3-3\Gamma) \quad (\text{B5})$$

The matrix $\mathbf{T}_{n[2/2]}^{\text{CC}}$ is stochastic. This property results from the fact that $\Gamma \leq 1$ and $P_2(-Y)$ do not have real roots.

References

1. G. A. Baker Jr. & P. Graves-Morris (1981), Pade' Approximants, Part I: Basic Theory, Encyclopedia of Mathematics and its Applications, Vol. 13, Addison-Wesley Publishing Company, London
2. V. Hristea & M. Pavelescu (1998), Green Transfer Matrix Method to Solving the S_N Transport Equation in (X,Y) Geometry: the Zero-th Order Momentum Approximation, Proceedings in the Annual Meeting on Nuclear Technology ' 98, pp 36, Munchen
3. V. Hristea & M. Pavelescu (1998) Local Galerkin' s Schemes Qualitative Analysis for 1D Transport Equation Solving, Ann. Nucl. Energy, Vol. 25, No. 13, pp. 1033-1053
4. V. Hristea (1999), The Green Function Used to Solve the Neutron Transport Equation, Ph.D. Dissertation (in Romanian), Bucharest University (I.F.A), Bucharest
5. E. E. Lewis & W. F. Miller, Jr. (1984), *Computational Methods of Neutron Transport*, John Wiley & Sons
6. H. Khalil (1985), A Nodal Diffusion Technique for Synthetic Acceleration of Nodal S_n Calculation, N. S. E., 99, 263-280
7. Ya. G. Sinai (1992), Probability Theory - An Introductory Course, Springer -Verlag, Berlin
8. W. F. Walters & R. D. O' Dell (1981), Nodal Methods for Discrete Ordinates Transport Problems in x, y - Geometry, Proceedings in the Advances in Mathematical Methods for the Solution of Nuclear Eng. Problems, Vol.1, pp 115-129, Munich.

9. X. Warin & J.-L. Vaurescal (1996), Study of Some S_N Nodal Methods in Neutron Transport, Technical Report, E. D. F. 1996, HI-72/95/017/0, Paris.